Available online at www.sciencedirect.com
ScienceDirect
Journal of the European Ceramic Society 29 (2009) 2447–2459
www.elsevier.com/locate/jeurceramsoc

# A new test to determine the tensile strength of brittle balls—The notched ball test

Peter Supancic *, Robert Danzer, Stefan Witschnig, Erich Polaczek, Roger Morrell

*Institut für Struktur- und Funktionskeramik, Montanuniversität Leoben, 8700 Leoben, Austria*

Received 26 February 2009; accepted 27 February 2009
Available online 18 April 2009

**Abstract**

A new strength test for ceramic spheres (balls) is presented. A long narrow notch is cut in the equatorial plane of the ball and the ball is then loaded in compression perpendicular to the notch. This causes tensile stresses in the outer surface region of the ball opposite to the notch, which are analysed carefully with finite element (FE) methods. The tensile stress amplitude depends on the bending moment in the notch ligament – given by the applied force – and on details of the notch geometry. The stress state in the highly stressed surface is almost uniaxial showing only a slight influence of Poisson's ratio. Numerical solutions for balls with quite different notch geometries are given.

Strength tests have been performed on commercial silicon nitride balls of 5 mm diameter. Two sets of specimens having notches of different length have been tested. Although the typical fracture loads in both sets of data are quite different, the tensile strengths are closely similar. This indicates the validity of the data evaluations. Experimental details are discussed and an analysis of the experimental uncertainties on the test results is made. For balls with 5 mm the uncertainties are estimated to be less than ±3% (of the measured value). For balls having a diameter of 10 mm or more the uncertainties are less than ±1%.


*Keywords:* Strength; $Si_3N_4$; Structural applications

## 1. Introduction

Silicon nitride ceramic balls have been used in high-performance, highly stressed bearing races for the last decade.[1] Compared with steel, silicon nitride has higher hardness, Young's modulus, wear and corrosion resistance, and a lower density, which are very beneficial for bearing applications. If used in electric power generation the high electrical resistance of silicon nitride makes electrical isolation via the bearing possible.[2] However, ceramic materials are more brittle than steels; therefore information on the strength of the balls is essential, but simple strength testing methods for balls are missing up till now.

Standard specifications exist for determining the properties of silicon nitrides for bearing balls,[3,4] but these require the strength of a candidate material to be determined using the usual four-point flexure test[5–7] on 3 mm × 4 mm × >45 mm test-pieces which generally have to be cut from specially prepared plate material fabricated in an identical manner, rather than from finished balls. For large balls (having a diameter of say 15 mm or larger) it is possible to machine bending specimens out of the balls in order to perform three- or four-point bending tests,[8] but this procedure is very costly. The surface of the specimens has to be prepared very carefully to avoid unrepresentative machining damage. Inevitably, in testing these specimens in bending the uniaxial tensile strength of the material is measured in materials originating from the interior of the balls with concomitant machining damage, but it should be noted that in bearing balls high tensile stresses only occur at and near their polished surface.

Disc shaped specimens can also be cut from the balls. Testing can be done by some kind of biaxial disc testing, e.g. using the ring-on-ring[9,10] or the ball-on-three-balls test.[11,12] This test can also be applied to specimens having only a few millimetres diameter. Again, specimen preparation is time consuming and costly, and as with the beam bending tests the interior of the ball material is tested. The preparation of the tensile loaded surface requires even more care than that of beam bending specimens, since under a biaxial stress state surface cracks of any direction

* Corresponding author. Tel.: +43 3842 402 4109; fax: +43 3842 402 4102.
*E-mail address:* phs@unileoben.ac.at (P. Supancic).

0955-2219/$ – see front matter © 2009 Elsevier Ltd. All rights reserved.
doi:10.1016/j.jeurceramsoc.2009.02.018

are possible fracture origins (in the case of uniaxial bending tests, cracks parallel to the stress direction are harmless).[13–15]

These classical methods of ceramic material testing thus do not reflect actual ball properties. Some work has been done to test whole balls by squeezing them together. This can be done by squeezing one ball between two plates, by positioning two balls one on top of the other and then squeezing them between plates, or even by positioning three balls on top of each other and then squeezing them between plates.[16] The first variety of this test is expected not to be very reliable; significant tensile stresses only occur in a ring shaped zone around the contact area between the plates and the ball (i.e. Hertzian stresses[17,18]). The highly stressed zone is very close to the area where the load is transferred from the fixture into the ball. Therefore the actual amplitude of the highest tensile stresses is sensitive to the details of the contact zone, e.g. some plastic deformation of the plates, the friction between the ball surface and the plates, surface roughness, or even some surface contamination. The loading situation is better defined in the second variety of this test, where the contact situation between the two balls is symmetrical and therefore free from friction effects. (Remark: by using spherical seats on the ends of the pistons the contact situation between the ball and piston is harmless with respect to failure initiation.) Therefore this type of test should be reliable if fracture starts near the middle plane. In the case of three balls, the situation for the ball in the middle is well defined on both contact regions and test results are significant, and reliable if fracture starts in the ring shaped near surface regions around the contact planes of the middle ball. This can be recognised by fractographic analysis of the broken pieces. However, the interpretation of the test results is still a little unclear. Recently, it has been claimed that this test does not determine the strength of the balls but is controlled by toughness and plasticity of the ball material,[8,19] and a similar conclusion was found recently for the contact loading of ceramic tools for metal forming.[20]

In this paper, a new strength test – the notched ball test – is proposed. A long and narrow notch is cut along the equatorial plane of the ball. The ball is loaded in compression along the axis perpendicular to this plane. High tensile stresses occur in the outer surface region of the ball opposite the notch root (in the ligament).[8] These stresses are used to determine the strength of the ball. Fracture starts from defects which exist in this region. It is important to note, that in this area the notched ball still has its original surface. Therefore notched ball test results are also a measure for the quality of the balls, i.e. of the ball surface preparation.

A similar test – the C-sphere test – was proposed in 2007 by Wereszczak et al.[21] In their test they used a wide notch with a fixed geometry; the notch length is 3/4 of the diameter, the notch width is equal to half of the diameter and the shape of the notch root is a semicircle. This notch geometry is used to maximise the effective surface of the specimen. But this wide notch is difficult and expensive to machine precisely. In our notched ball test a narrower notch is used, having a typical width between 5 and 20% of the diameter and a typical length of 75–90% of the diameter. The exact geometry of the notch root (e.g. half circle, rectangular, etc.) can be determined after machining and is used for the determination of the stress field. These notches can be machined using simple commercially available grinding wheels.

## 2. Analysis of the stress field in the notched ball specimen

### 2.1. Overview

In this section, the stress field of ideally notched balls is described. All examples shown here are based on spheres with a diameter of $D = 5$ mm and for a material with Poisson's ratio $\nu = 0.27$ corresponding to that of the $Si_3N_4$ balls tested experimentally. However, the results can be generalised by scaling with the diameter of the spheres and a simple formula to calculate peak stresses given by the applied force will be derived (similar to the evaluation of a bending test). The general feature of this type of notched ball test is a narrow notch cut into a sphere along the equatorial plane. A schematic sketch of the testing arrangement and the definitions of the geometric parameters are given in Figs. 1 and 2.

A finite element (FE) model has been programmed within the framework of ANSYS® classic, version 11SP1.[22] The whole model is built up parametrically by programming an input code with the programming language APDL (APDL: Ansys Parametric Design Language[23]), and uses pure hexahedra elements. Highly stressed regions are meshed with smaller elements (i.e. the region within and around the ligament behind the notch base), while other parts of minor interest and low stress gradients have larger elements (see Fig. 2).

The middle plane of the notch (i.e. plane of symmetry) is defined to be the $X$–$Y$ plane. The base of the notch root is parallel to the $Y$-axis. The force is applied parallel to the $Z$-axis at the poles of the sphere, see arrows in Fig. 1. The $X$–$Z$ plane is also a plane of symmetry; therefore only a 1/4 model is needed to describe the problem (for the case of the ideal arrangement).

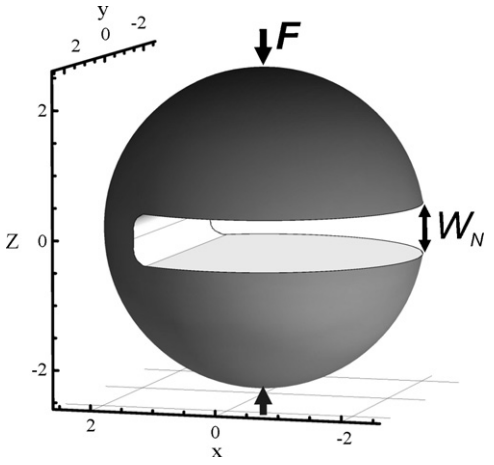


Fig. 1. Sketch of the testing arrangement: the notched ball ($D = 2R = 5$ mm) is loaded perpendicular to the equator plane at the poles, see arrows. The axes shown define the Cartesian coordinate system used. The origin is the center of the ball. $W_N$ is the width of the notch. The other geometric parameters are described in Fig. 2.

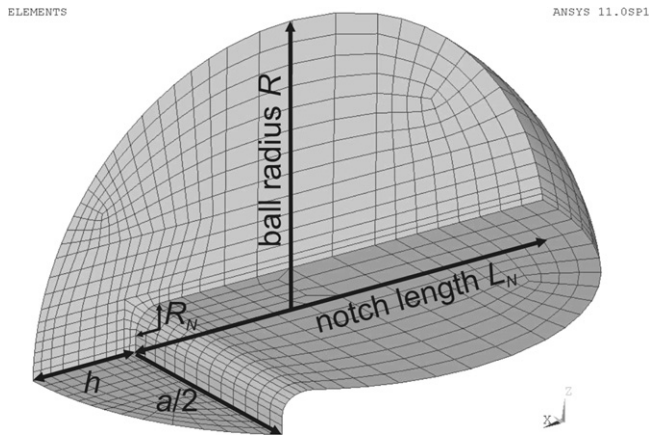


Fig. 2. The mesh of a notched ball specimen (quarter model). For the purposes of clarity the plotted mesh is relatively coarse. The meshes used for the calculations are much finer and have up to one million nodes. The remaining ligament on the $X$–$Y$ plane has the maximum thickness $h = D - L_N$. Its length $a$ depends on the ball radius $R$ and the notch length $L_N$.

The stress field in the (ideal) ball specimen depends on the ball radius, $R$ (diameter: $D$), the notch length, $L_N$, the notch width, $W_N$, and the radius of the fillet $R_N$ of the notch base, which are defined in Figs. 1 and 2. The stress field is not uniaxial. Therefore it also depends on Poisson's ratio, $\nu$ (note: within the linear-elastic approach the stress is independent of Young's modulus, since the experiment is force driven). Of course, the stress also depends on the applied force, $F$. In total these are six independent parameters. To generalise the results the definition of the following dimensionless geometric parameters is convenient: the relative notch length $\lambda = L_N/D$, the relative width of the notch $\omega = W_N/D$, and the relative radius of the fillet of the notch base $\rho = R_N/W_N$. (Remark: the domain of the relative fillet radius is $0 \leq \rho \leq 0.5$; 0 corresponds to a rectangular, sharply cornered notch root.)

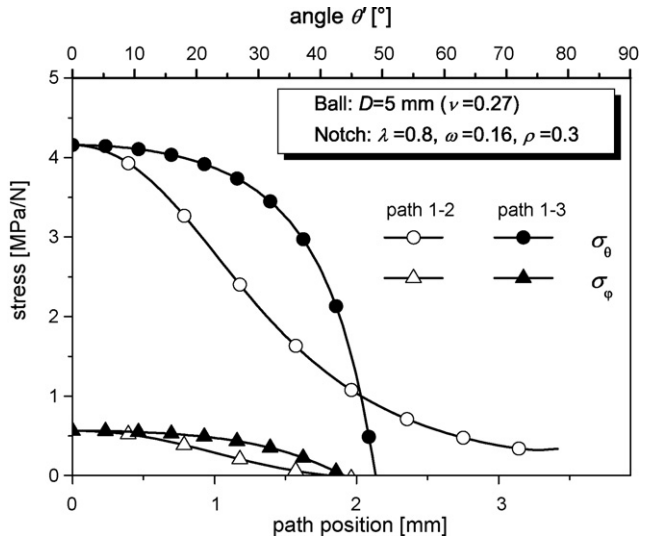


Fig. 4. Course of the first and second principal stresses (i.e. $\sigma_\theta$ and $\sigma_\varphi$) along the equator line (i.e. paths 1–3, compare Fig. 3), and along the great circle perpendicular to the equator plane (i.e. paths 1–2). The second principal stresses are small compared to the first ones. The angle $\theta'$ is measured between position 1 and the corresponding point on a certain path with respect to the center of the ball. In case of describing paths 1–2, it is a vertical angle, while in case of paths 1–3 it is an horizontal angle (identical to the polar angle in the spherical coordinate system).

An example of the stress field in a typical notched ball specimen is shown in Fig. 3. The distribution of the first principal stress is plotted on the surface (left) and on the planes of symmetry (right) of the specimen. The used parameters are given in the figure caption. It should be noted that in the loading range of interest the stress field linearly scales with the applied force, $F$.

Significant tensile stresses arise in and near a relatively large surface area in the ligament opposite the notch. Fig. 4 shows

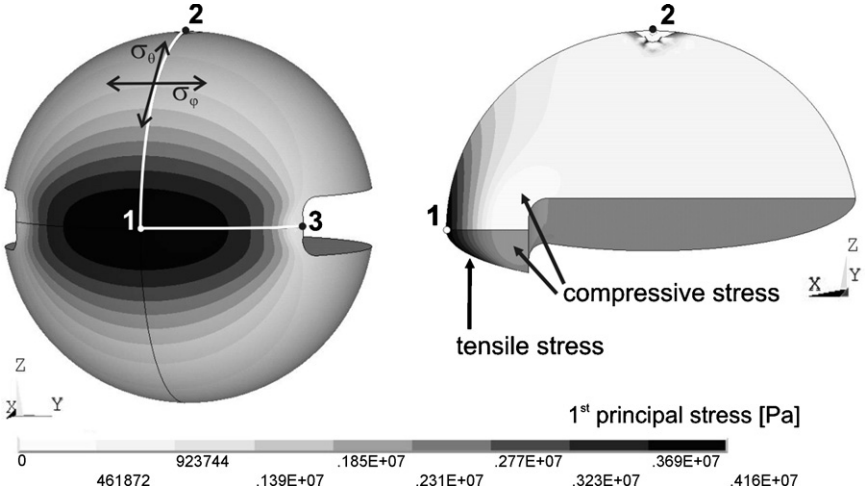


Fig. 3. Distribution of the first principal stress in the notched ball specimen (left: tensile stressed region at the surface of the ball; right: view on inner regions according the planes of symmetry on a quarter model). The parameters used are: $D = 5$ mm, $L_N = 4$ mm, $W_N = 0.8$ mm, $R_N = 0.24$ mm. For the elastic constants, typical data of a silicon nitride material are used ($E = 300$ GPa and $\nu = 0.27$). The applied force is $F = 1$ N. The tensile stresses concentrate in the ligament opposite the notch base. The maximum of the first principal stress (peak stress) is at position 1. The tensile peak stress is 4.16 MPa/N. The black double arrows indicate tangential stresses with respect to both directions, namely the azimuth $\varphi$ and polar angle $\theta$ (defined in a spherical coordinate system). At point 1 the maximum stress direction is parallel to the $Z$-axis (identical to $\sigma_\theta$).

the course of the first and second principal stresses (identical to $\sigma_\theta$ and $\sigma_\varphi$) along the equator line (path from 1 to 3; see Fig. 2) and along the great circle perpendicular to the equator line (path from 1 to 2) for the relative fillet radius $\rho = 0.3$. Stresses higher than 90% of the tensile peak stress occur in a relatively large region (in the case shown in Figs. 3 and 4 this regime goes from $-27^\circ$ to $+27^\circ$ along the equator line and from $-12^\circ$ to $+12^\circ$ along the great circle perpendicular to the equator). Outside this region the stress amplitudes strongly decrease. Near the contact point (at the poles of the sphere) the stress amplitude steeply increases and becomes singular. But this singularity is an unrealistic consequence of the point loading model used in this analysis. Taking a realistic contact situation into account the singularity would not occur. Since the load transfer occurs far from the ligament region these details of the modelling of the contact are not relevant for the stresses in the ligament.

Also shown is the course of the second principal stress. It can be recognised that it is much smaller than the first principal stress. In fact in the ligament opposite the notch the stress state is almost uniaxial and resembles that of a bending bar. Therefore the influence of Poisson's ratio on the maximum value of the stress is very limited. For the case analysed in Figs. 3 and 4 Poisson's ratio of 0.20 (instead of 0.27) would cause a peak tensile stress of 4.19 MPa (instead of 4.16 in the case of Fig. 3). For typical range of Poisson's ratios of ceramic materials (i.e. 0.2–0.3) the variation of the stress amplitude is therefore smaller than 1%.

In the region around the notch root only compressive stresses occur. This fact is of great practical relevance. In this area some machining damage caused by specimen preparation is inevitable. However, this damaged region is not stressed in tension, so such damage will have no relevance for the notched ball test results.

In the following section the influence of the notch geometry on the stress field will be discussed.

### 2.2. *Influence of the length, the width and the fillet radius of the notch*

The stress field in the ligament resembles that of a bent beam, where the tensile stress scales with the square of the height of the beam. Similar behaviour can be expected for the notched ball test geometry. Here the height corresponds to the ligament thickness $h$ (see Fig. 2). It can therefore be expected that the ligament thickness $h = D - L_N$ (or the notch length, respectively) will be the most prominent geometric parameter for the amplitude of the stress field.

Fig. 5 shows an evaluation of the principal stress at the equator plane (i.e. at position 1) versus the notch length for several combinations of notch width and fillet radius. The force (1 N) and Poisson's ratio (0.27) are kept constant. A steep increase of the stress with increasing notch length (i.e. decreasing ligament thickness) can be recognised. It is approximately inversely proportional to the third power of the ligament thickness. By comparison, the influence of the other parameters (notch width and fillet radius) on the tensile stress is weak.

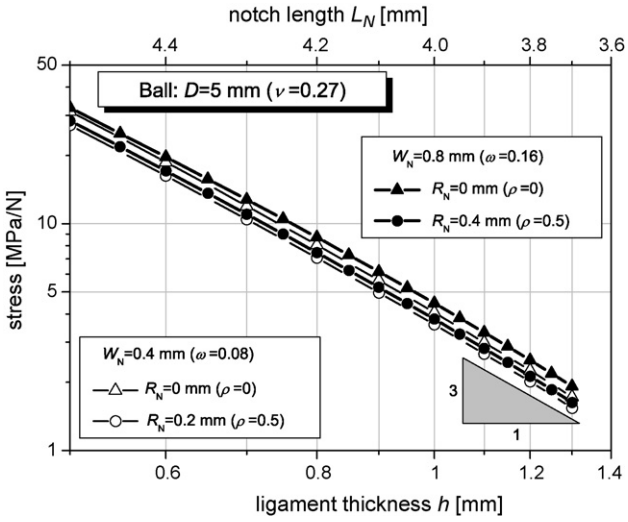


Fig. 5. The maximum of the first principal stress at the equatorial plane (at position 1) versus the ligament thickness in a double logarithmic scale for several combinations of widths and fillet radii of the notch. The applied force is 1 N and Poisson's ratio is 0.27. The (normalised) stress amplitude approximately depends on the (−3)rd power of the ligament thickness.

For a very deep notch ($\lambda = 0.9$) the course of the first principal stress along the great circle perpendicular to the equator (notch) plane (paths 1–2) is shown in Fig. 6. The varied parameter in this plot is the fillet radius. If it is half of the notch width a continuous decrease of the tensile stress from the equator to the pole occurs. The maximum of the first principal stress at the equator plane is at position 1. It is also the tensile peak stress in the specimen. But if the fillet radius is small (e.g. if it is 0) and if the notch width is wide enough the tensile peak stress occurs a little above (and below) the equatorial plane, i.e. the tensile peak stress in the specimen is no longer at position 1 in the equatorial plane.

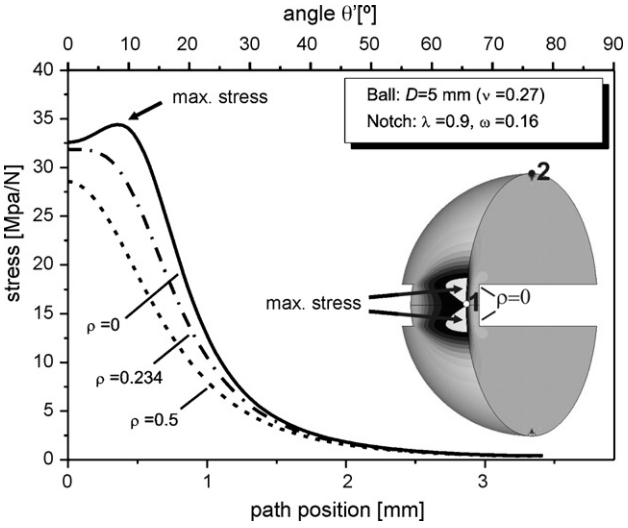


Fig. 6. Course of the first principal stress along the great circle of the sphere perpendicular to the equator (from 1 to 2). The curves are for three values of the relative fillet radius of the notch. The applied force is 1 N and Poisson's ratio is 0.27. Note that with small fillet radii the peak stress position moves from the equatorial plane and splits into two maxima. The insert shows the stress field for a fillet radius of 0.

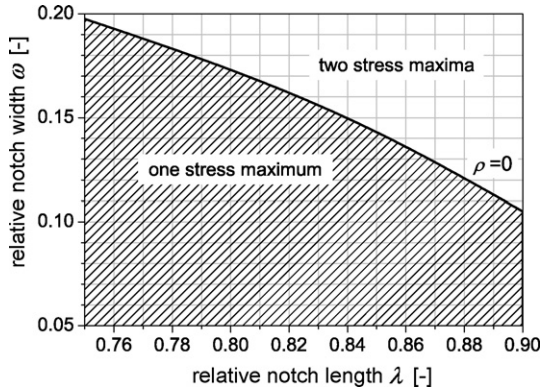


Fig. 7. Transition line between the regime with two and with a single maximum of the first principal stress as a function of relative notch width and relative notch length. Poisson's ratio is 0.27 and the relative fillet radius is $\rho = 0$. For larger relative fillet radii the transition line would shift upwards. For $\rho = 0.5$ only the "one stress maximum" regime exists.

This situation is promoted by the fact that for wide and sharp notches the minimum of the ligament thickness does not occur at the equatorial plane (as for round notches) but occurs opposite the two edges of the sharp notch. The curve for the intermediate fillet radius (i.e. $\rho = 0.234$ which is $R_N = 0.188$ mm for this ball size) corresponds to the borderline between the regions with one and two maxima.

It can be recognised that the size of the area with almost constant stress amplitude is largest near that borderline. For strength testing situations spatially constant stress states are beneficial. Therefore notch geometries near this borderline are recommended for notched ball specimens (but other geometries can also be used and evaluated; details are described later). For the following data evaluations the stress amplitude at position 1 is used for the determination of strength.

The boundary between the two-maxima region and the single-maximum region is shown in Fig. 7 as a function of relative notch width and relative notch length for a Poisson ratio of 0.27. The borderline shows the situation for a sharp rectangular notch (fillet radius $\rho = 0$). It can be immediately recognised, that wide and deep notches promote the two-maxima regime. This regime is also promoted by small fillet radii and does not occur for large fillet radii, i.e. for $\rho = 0.5$.

In the following the first principal stress at position 1 is used for the determination of strength, as is the convention in all other ceramic mechanical testing. A general assessment for this stress will be given in the next section.

### 2.3. A general solution for notched ball specimens

As shown in the previous sections, high tensile stresses occur only in the region of the remaining ligament behind the notch base. Apart from the applied force, the size of the cross-section of the ligament, which is given by a circle segment (see Fig. 2), plays a major role in determining the tensile stress amplitude.

To derive a simple formula for calculating the tensile stress amplitude with respect to the applied force and geometry of the specimen, the approach of beam theory is used in a modified way. Actually, the loading situation in a notched ball specimen is similar to that in a beam with a given cross-section (i.e. circle segment) loaded by the superposition of a torque $M_y$ and a compressive stress (negligible in a first-order approximation), which both are proportional to the force (see Fig. 1 and Appendix A). As a rough approximation within the regime of parameters used in this work, the tensile stress amplitude $\sigma$ is given by

$$\sigma \approx \frac{6F}{h^2}. \tag{1}$$

This equation is useful for quick estimations of the tensile stress at position 1. Note that the stress amplitude does not depend on the ball size directly; it depends on the ligament thickness $h$, which is, of course, related to the ball diameter in order to stay in a regular parameter range.

A more accurate expression for the stress amplitude can be described by

$$\sigma = f_N \frac{6F}{h^2}, \tag{2}$$

where a dimensionless correction factor $f_N$ accounts for the deviations of the approximate expression in Eq. (1). The function $f_N = f_N(\lambda,\omega,\rho,\nu)$ depends on the relative notch length $\lambda = L_N/D$, the relative notch width $\omega = W_N/D$, the relative radius of the fillet $\rho = R_N/W_N$ at the notch base and on Poisson's ratio $\nu$. This function has been determined numerically on the basis of several hundreds of FE-calculations in the parameter ranges which are of interest for the notched ball test:

$$0.75 \le \lambda \le 0.92, \qquad 0.05 \le \omega \le 0.20, \qquad 0.00 \le \rho \le 0.50,$$
$$0.20 \le \nu \le 0.30. \tag{3}$$

The factor $f_N$ increases with increasing notch length. In the parameter range of interest it is between 0.4 and 1.5. It is plotted in Fig. 8 versus the relative notch length for several combinations of relative width and relative fillet radius of the notch. Poisson's ratio is selected to be 0.27.

A power series for the evaluation of $f_N = f_N(\lambda,\omega,\rho,\nu)$ has been fitted to the numerical results of the parametric study. The fit function describes the data gained by the numerical analysis with an error less than 1%. The analysis has also been used to

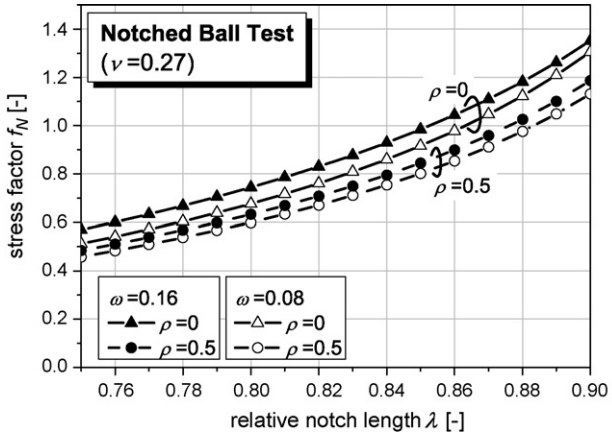


Fig. 8. Dimensionless factor $f_N$ versus the relative notch length λ for several combinations of relative widths and fillet radii of the notch. Poisson's ratio is 0.27.

check the published results for the C-sphere test.[21] Our results and the results published for this geometry match within 0.5%. However, the full power series has more than 50 terms and it is inappropriate to publish it in the present paper (in the near future, the full formula will be published at our homepage[24]).

For the notched ball specimens used in the experimental part of this paper ($\omega = 0.13$, $\nu = 0.27$, $0.75 \leq \lambda \leq 0.85$, $0 \leq \rho \leq 0.5$), a simplified analytical expression for $f_N$ for this range of parameters is given below:

$$f_N(\lambda, 0.13, \rho, 0.27) = -0.400 + \frac{(0.083042 + 0.5740\lambda - 0.4300\lambda^2)(1 - 0.085\rho)}{(1 - 0.9535\lambda + 0.0503\rho^2)} \quad (4)$$

In summary, with the results described above, the full characterisation of the stress state in notched ball specimens becomes possible.

## 3. Experimental work

### 3.1. Test procedure

Commercial silicon nitride balls with a diameter of 5.00 mm were used for this investigation. Young's modulus of the material is $E = 310$ GPa and Poisson's ratio is $\nu = 0.27$.

Specimen preparation was made in batches. Each batch of balls (in this case 27 and 32 specimens, respectively) was carefully glued (crystalbond™ 500) in a specially designed guide rail (see Fig. 9). This arrangement is made to ensure that the notches are in the equatorial plane of the balls and that the length of the notch in the batch is consistent. Special care was taken to not damage the surface area of the balls opposite the notch (in the ligament). At one end of the row of balls a rectangular plate of the same silicon nitride material was also fixed in the guide rail perpendicular to the row direction. Then the notches were machined into both balls and plate in one single operation step using a commercial diamond impregnated grinding wheel. In the present case a wheel with a nominal width of 0.6 mm was used. The grinding wheel was redressed to a square edge after machining each notch. It is assumed that the notch in the flat end-plate is representative of the notches in all the balls of the batch. The width and fillet radii of the notches were determined on the notch in the plate. Two different classes of notch lengths were machined (with about 78 and 82% of the ball diameter), giving two sets of specimens having different regimes of fracture load.

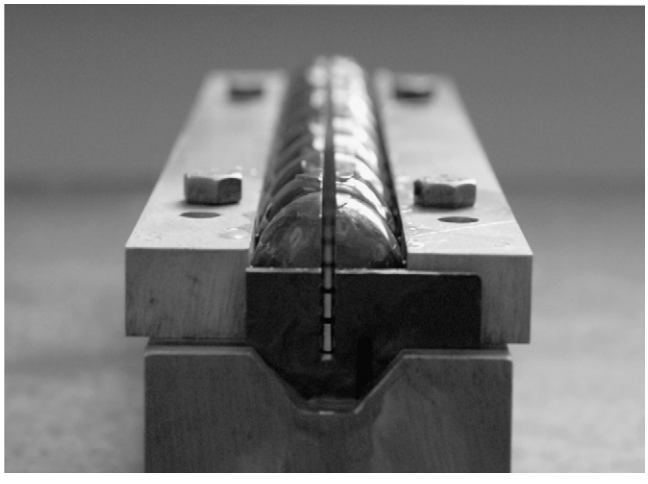

Fig. 9. The notch in a row of ball specimens glued in the guide rail seen after machining. The plate at the end of the row of balls can be recognised.

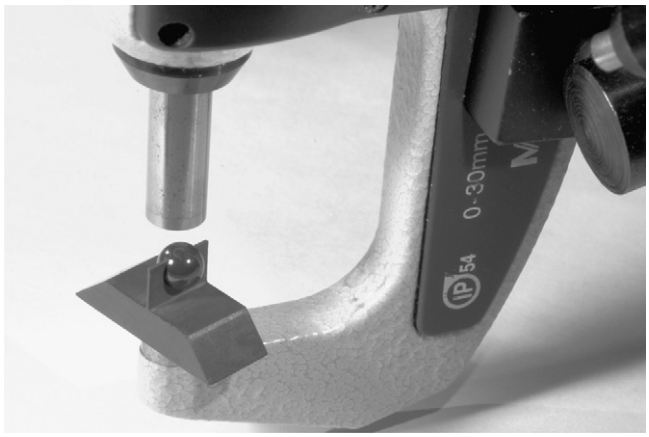


Fig. 10. Arrangement to determine the notch length (ligament thickness). The thickness of the measuring blade is adjusted to the notch width. The tip of the blade is sharpened, so that the blade can reach the notch root even if the corners of the notch are rounded. The measurement aid is positioned between the callipers of the micrometer screw. Measured is the difference between the edge of the blade and the top position of the ball.

After machining, the glue was removed by a thermal treatment (ca. 140 °C) in a simple air furnace. The samples were then cleaned in acetone and were then ready for the determination of the notch geometry. The notch length of each individual ball was measured individually. For that a special measuring tool was developed (see Fig. 10), which makes the use of a conventional screw micrometer calliper possible. It is considered that the measuring error is smaller than ±5 μm, i.e. the notch length can be determined with a relative error of about ±0.1% or less, and hence and the ligament thickness with an error of about ±0.5% or less (if the ligament thickness is about 20% of the ball diameter). The individual values for the ligament thickness are later used for the evaluation of strength. In any event, a check can be made by measuring the width of the fracture surface after fracture.

The measurement tool was also used to determine the position of the notch in relation to the equatorial plane. For that, the tool was rotated for 90° to leave the blade horizontal and was then fixed in that position. The specimens were placed on the blade of the tool, and the distance between the notch face and the ball pole, position 2, was measured. Then the specimen was turned around and the distance of the other notch face to the position of the pole opposite to position 2 was measured. The deviation of the notch plane from the equatorial plane is half of the difference between the two distances. In practice, it was less than ±20 μm using careful set-up in machining.

The width and the radius of the fillet at the notch root were determined on the notched end-plate by light microscopy (see

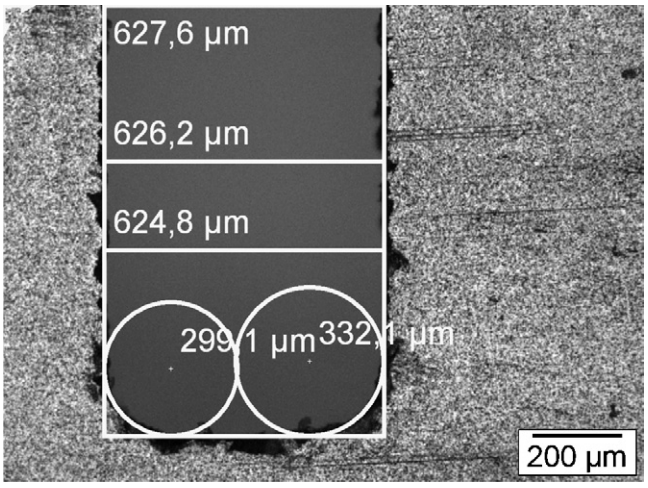


Fig. 11. Notch width (625 ± 5 μm) and the radius of the fillet at the notch base (300–330 μm) were determined with an optical microscope.

Fig. 11). It is assumed that the notch geometry of the balls of each batch is equal to that of the end-plate. The notch geometry was determined for each batch separately. The measurement uncertainty of the width is estimated to be ±10 μm or less. In the case considered here, the notch width is 625 ± 5 μm; i.e. the relative uncertainty is about ± 1% or less.

The measurement of the fillet radius is also indicated in Fig. 11. Here the estimated uncertainty is ±30 μm; i.e. the relative uncertainty is about ±5% of the notch width.

Next, the specimens were fractured using a universal testing machine. The specimens were placed between the two parallel faced rams. The end-plates of these rams were made of hardened steel. After the testing some indents similar to Brinell indents could be observed in the steel plates. Therefore some friction cannot be excluded. A few additional tests were made in fixtures with silicon nitride loading platens in order to reduce indentation and frictional effects. No significant influence of friction on test results could be detected. However, for a clear assessment of this problem more experiments would be necessary. Clearly, to minimise any possible effect of frictional effects, it is recommended that silicon nitride platens should be used.

The notch was aligned perpendicular to the direction of load application using a positioning aid (Fig. 12). The angular alignment of the equatorial plane is much better than ±1°. Then a preload is applied (about 10% of the estimated fracture load), and the positioning aid is removed. The load is increased at a rate such that fracture occurs within 10 s to 1 min. After the strength tests a fractographic analysis of selected fracture surfaces has been performed.

### 3.2. Error analysis

For the validation of experimental results an analysis of measurement uncertainties is essential. In this section the uncertainties for the determination of the fracture stress are analysed. The tensile stress at position 1 (which is used to determine the strength of the balls) depends on five parameters (Eq. (2)): $F$, $\lambda$, $\omega$, $\rho$ and $\nu$. The relative length parameters also depend on the ball diameter $D$.

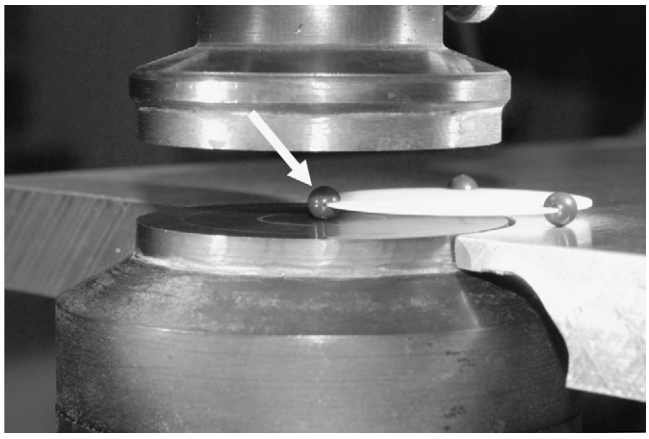

Fig. 12. The specimen (marked by an arrow) is aligned perpendicular to the loading direction with the use of a simple positioning aid.

Of course, the measuring uncertainty depends on the size of the specimens. In the following the analysis is made in detail for balls with a diameter of 5 mm. Later the uncertainties for other ball sizes will briefly be discussed.

*Diameter*. The diameters of the balls are determined with an accuracy of ±2 μm using a conventional micrometer calliper. For balls having a diameter of 5 mm or larger, the corresponding measurement uncertainty is less than ±0.04%. The influence on the determination of strength is much smaller than 0.4%.

*Force determination*. Following Eq. (1) and for ceramic balls having strength of 100 MPa or more the expected fracture load is 4 N or more (see Eq. (1) for $h = 0.25$ mm). With a typical universal testing machine equipped with a load cell of class 1[25,26] a measurement error for the force of less than 1% can be expected. The force enters linearly into the determination of strength. Therefore the measurement uncertainty due to the force measurement by a calibrated load cell is less than 1% of strength.

*Friction effects*. Friction between the balls and the hardened steel plates of the pistons in the testing machine cannot be completely excluded. But we believe that the influence of friction on strength is small, in any case smaller than the inherent scatter of the data. In any case friction would cause a (small) systematic overestimation of the strength, which is not taken into account in our data evaluation. In future experiments friction can be avoided by the use of silicon nitride end-plates.

*Poisson's ratio*. In general Poisson's ratio is not precisely known but its influence on the stress at position 1 is negligible. To give an example, if the relative measurement uncertainty of Poisson's ratio is ±5%, its influence on the determination of the stress is far less than ±0.1%.

*Notch length and ligament thickness*. We believe that the measurement of the length of the notch (and of the ligament thickness) can be made with an accuracy of ±5 μm or better using a conventional micrometer calliper and the measuring aids described above. The essential step before the measurement is that the notch has to be cleaned carefully. For balls with a diameter of 5 mm and a very long notch length of 4.5 mm the precision

Table 1
Strength test results gained on notched ball specimens. The ball diameter is 5.000 ± 0.001 mm and the Poisson ratio is 0.27. Numbers in round brackets are in relative units (geometric data) and numbers in square brackets refer to the limits of the 90% confidence intervals resulting from the sampling procedure (Weibull parameters), see Ref. [30].

| | Set A | Set B |
|---|---|---|
| Notch length, $L_K$ (mm) ($\lambda$) | 4.165–4.070 (0.81–0.83) | 3.885–3.968 (0.77–0.79) |
| Ligament thickness, $h$ (μm) ($h/D$) | 835–930 (0.17–0.19) | 1032–1115 (0.21–0.22) |
| Notch width, $W_N$ (μm) ($\omega$) | 630 ± 10 (0.126 ± 0.002) | 630 ± 10 (0.126 ± 0.002) |
| Fillet radius, $R_N$ (μm) ($\rho$) | 130 ± 20 (0.206 ± 0.03) | 130 ± 20 (0.206 ± 0.03) |
| Fracture force range (N) | 180–276 | 333–475 |
| Characteristic strength (MPa) | 1343 [1304–1384] | 1336 [1303–1370] |
| Weibull modulus | 12.1 [8.9–14.9] | 12.9 [9.8–15.7] |

of notch length measurement is about ±0.1%. The corresponding measuring uncertainty for the ligament thickness is therefore ±1%. The influence on the determination of strength is less than ±3%. It should be noted that the ligament thickness varies from specimen to specimen and a precise determination of the ligament thickness is of the highest relevance for the precise determination of strength.

*Notch width*. The determination of the width of the notch is done after machining in an optical microscope. It can easily be determined with an accuracy of ±5 μm or less. Since the notch width has only a minor effect on the tensile stress at position 1 the corresponding measuring uncertainty for the strength is as small as ±0.1%.

*Fillet radius*. The radius of the fillet of the notch base results from the wear of the grinding wheel and has to be determined in an optical microscope after machining of the notch. Measurement uncertainties are relatively large, i.e. they may be of the order of ±30 μm. For notches having a width of 300 μm (accurate thinner notches are difficult to machine using conventional grinding wheels) the corresponding relative uncertainty is about ±7%. Following Eq. (2) this would result in a measurement uncertainty for the stress of about ±3%. Of course, for wider notches, the relative error is smaller.

*Alignment of the specimen*. This is made with a positioning aid as shown in Fig. 12. The thickness of the blade of the positioning aid is only a little smaller than the width of the notch (in the order of 10 μm). The resulting twisting and tilting of the ball depend on the size of the ball and the length of the notch. For 5 mm balls this would result in a maximal tilting angle of less than ±1°. An FE-calculation was made to analyse the influence of this angle on the stress value. It results in an uncertainty of much less than ±0.1% of the determined stress value.

*Offset of the notch*. The former analyses were made for geometrically ideal notched ball specimens. However, it is possible that the notch is not machined exactly along the equatorial plane of the ball and that there exists a small offset. For a 5 mm ball having a notch width offset of 200 μm (4% of the diameter) an FE-calculation was made. It increased the ligament stress amplitude by 2.8%. The actual offset has been determined in these experiments less than 20 μm and the resulting measuring uncertainty in stress is much less than 0.5%.

In summary, in the case of the 5 mm balls there are two situations which may cause large measurement uncertainties: if very deep notches are machined into the balls (i.e. $\lambda > 0.9$) the ligament is very thin and uncertainties in the ligament measurement may cause uncertainties in the stress determinations up to ±3%. In the case of very narrow notches uncertainties in the measurement of the fillet radius may cause uncertainties in the stress determinations about ±2%. Furthermore the determination of the fracture load may have uncertainties up to ±1%. In the case of the experiments described in the next section, the notches were not so deep and narrow and the uncertainties due to ligament and fillet radius measurement are much smaller than in the extreme case discussed above. We believe that in this case the overall measurement uncertainty is about ±2%.

From the practical point of view the applicability of this test will be restricted by the ability to machine precise notches into the balls. Using typical facilities of a well equipped machine shop this will hardly be possible for balls with a diameter much smaller than 2 mm. For balls having a diameter of 2 mm the uncertainties will be dominated by the uncertainties in the measurements of the ligament thickness. For very deep notches the corresponding uncertainties in the determination of the strength can be up to ±10%, but for notches with a length of say 1.5 mm it is much less (about ±4%).

For much larger balls having a diameter of 10 mm or more all measurements concerning the geometry of the balls and the notches become simple and the overall measurement uncertainty is given by the uncertainty of the load cell.

### 3.3. Experimental results

A summary of the strength results is given in Table 1, which includes the geometric parameters of the two sets of notched ball specimens, the mean fracture loads and the Weibull parameters[10,27–29] of the sets. The data evaluation was made according to Ref. [30]. The corresponding Weibull distributions[10,28] for the fracture load and the fracture strength are shown in Fig. 13.

It can clearly be recognised that the fracture loads of each set are quite different but the strength is not. Within the 90% confidence limits the strength data of the two sets are equal.

A typical pair of matching fracture surfaces is shown in Fig. 14. The fracture origin can clearly be recognised. A distribution of the positions of fracture origins and the distribution of the first principal stress along the equator line are shown in Fig. 15. No failures occurred associated with the machining damage at the end of the ligament.

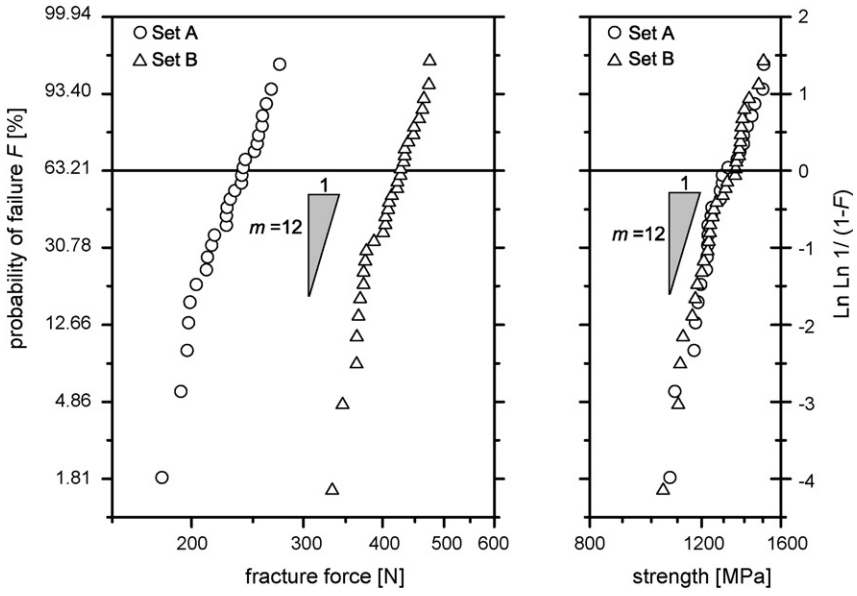


Fig. 13. Weibull distributions of the two sets of specimens. Probability of failure (a) versus fracture load and (b) versus strength. The strength of the two data sets is equal.

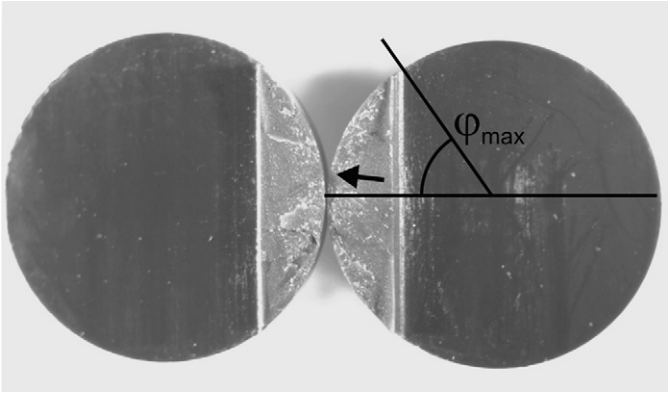


Fig. 14. Matching pair of fracture surfaces. The fracture origin is marked by an arrow. Also shown is the definition of the azimuthal angle $\varphi$ to define the positions of fracture origins ($\varphi = 0$ is the direction given by the vector between the center of the ball and position 1, see Fig. 3).

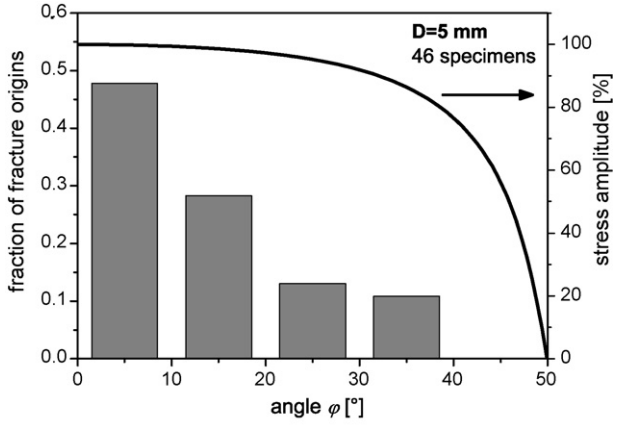


Fig. 15. Angular distribution of fracture origins (see definition of the azimuthal angle in Fig. 14). Also shown is the slope of the stress along the equator line (i.e. positions 1–3, see Fig. 3).

## 4. Discussion

The procedure to manufacture the notched ball specimens and to perform the test is relatively simple. Even for the balls with a diameter of 5 mm, which are relatively small for strength specimens, the notch can – using typical equipment of a machine shop in a ceramic institute – be machined with such a high precision, that the measurement uncertainties resulting from geometrical inaccuracies are in the order of 2% of strength or less. This is comparable with the uncertainties in standardised bending tests.[31,32]

We believe that testing of even smaller specimens is possible, e.g. of specimens having a diameter of 2 mm. But in this case the exact machining of the notches becomes demanding and the exact measurement of the ligament thickness will be difficult. The strongest influence on the tensile stress maximum has the ligament thickness (to about the negative third power). A small uncertainty in the ligament thickness can cause a large uncertainty in stress. Relative uncertainties of the ligament thickness become smaller as the ligament thickness is increased. Therefore – at least for small balls – we recommend as large ligaments as possible, i.e. with a thickness of 25% of the diameter (the numerical analysis has not been made for thicker ligaments). The corresponding notch length is about 75%.

For balls with a diameter of 10 mm or larger the measurement uncertainties become very small, i.e. 1% of strength or even less. For these tests the limiting factor concerning precision is the force measurement. It is quite obvious that for these specimens the notched ball test is more precise than a standardised bending test.[31,32]

The analysis of the fractured specimens showed that all fracture origins were at or very near the surface (see Fig. 14). This is consistent with the stress distribution in the specimens. The distribution of the fracture origins over the equator is also consistent with the angular stress distribution (see Fig. 15). Although

a detailed study has not been performed in the actual case, we know from our work on larger bearing balls, that fracture origins often are some kind of surface damage, which – in most cases – is caused by the machining or by the handling of the balls. To avoid additional surface damage in our notched ball specimens produced during the machining special care was given to protect the surface area opposite the notch. To give some examples handling of the balls was made by a pair of polymer tweezers. During the grinding the balls were glued into a V-shaped notch, and the surface opposite the notch was protected by soft glue. The specimens were stored in small individual boxes made of soft materials. We are quite sure that our precautions were successful and no surface damage was caused by our handling or machining.

Two sets of notched ball specimens were machined and tested in this work. They derive from the same production batch. The machined notches had almost the same width (relative width 12.6%), fillet radius (relative radius 21%) but some scatter in the length (and in ligament thickness). In the first batch the ligament thickness ranged from 835 to 930 μm (relative thickness 16.7–18.6%) and in the second batch from 1032 to 1115 μm (relative thickness 20.6–22.3%), i.e. the variation of the ligament thickness in each set is about ±5%. Uncorrected this would have a serious influence on the determined strength (about ±15%), and so should be taken into account in the data evaluation. Therefore the individual ligament thickness of each individual specimen has to be determined and accounted for in the stress determination. If this variation is not to be taken into account each strength test would have an uncertainty in strength of about 15%. However, if an average ligament thickness were to be used in the determination of the mean or the characteristic strength there would be no effect. By comparison, the fracture force (see Table 1) in each set is scattered by about ±25%.

In Fig. 13 the data are plotted in Weibull diagrams[10,15,30] for the fracture load and strength, respectively. Both diagrams are plotted on the same relative scale. The data are quite well arranged along straight lines, i.e. they are well described by Weibull distributions.[15] The slope of the lines is the Weibull modulus, which is a measure for the scatter of data. It is almost equal in both types of plots, although in the "force Weibull diagram" the influence of the scatter of the ligament thickness (about ±5% of the ligament thickness and about ±15% in strength) is not taken into account and in the "strength Weibull diagram" it is. It is surprising to note that in the "strength Weibull diagram" the influence of the scatter of the ligament thickness is completely masked by the wider inherent scatter of strength data (about ±25%). We had expected that the force distribution would be wider than the strength distribution, because it results from the superposition of the inherent strength distribution with the scatter of the ligaments. However, this behaviour is typical for the superposition of wide and narrow distributions.

Both sets of specimens differ in the mean ligament thickness; in the second set it was 20% larger than in the first set. Therefore the mean fracture load was also larger (by 77%), see Table 1 and Fig. 13. But the strength distributions of both sets are almost equal. This is a strong hint that the quality of the data analysis is quite good.

Weibull distributed data show a dependence of strength on the specimen size.[10,15] The larger the specimen, the higher is the probability of finding a large flaw, which causes a low strength. If the failure is initiated by volume flaws, for a uniaxial stress state the size effect on strength is given by[10,15]

$$\sigma_1 = \sigma_2 \left( \frac{V_{eff,2}}{V_{eff,1}} \right)^{1/m}. \quad (5)$$

The indices refer to specimens with a different size and/or geometry. The Weibull modulus is $m$. The effective volume of the specimen is defined by

$$V_{eff} = \int_{\sigma>0} \left( \frac{\sigma}{\sigma_0} \right)^m dV. \quad (6)$$

The integration is made over volume elements, where the stress is tensile (i.e. positive). In general, $\sigma_0$ is an arbitrary normalising factor. We chose it to be equal to the tensile peak stress at the equator plane. If a general stress state is applied the stress has to be replaced by a suitable equivalent stress. Often the principle of independent action is used:

$$\sigma_{eq}^{PIA} = (\sigma_I^m \cdot \Theta(\sigma_I) + \sigma_{II}^m \cdot \Theta(\sigma_{II}) + \sigma_{III}^m \cdot \Theta(\sigma_{III}))^{1/m}, \quad (7)$$

where $\sigma_I$, $\sigma_{II}$, $\sigma_{III}$ are the principal stresses. The action of compressive stresses is neglected, which is taken into account by the use of the Heaviside-function $\Theta$. For details see Refs. [10,15].

In the case of notched ball specimens the first principal stress is large compared to the other stress components, and – since $m \gg 1$, it holds that: $\sigma_{eq}^{PIA} \approx \sigma_I$, i.e. the fracture behaviour is triggered by the first principal stress.

If fracture is caused by surface flaws (as in the case described here) analogue definitions can also be made for the effective surface. Fig. 16 shows the effective volume and the effective surface of the specimens of sets A and B as a function of the Weibull modulus. The influence of the different notch lengths ($\lambda = 0.82$ or 0.78, respectively) on the effective volume (surface) is roughly a factor of 2. The effective volume of the notched ball specimens for a Weibull modulus of $m = 12$ is about 0.3 or 0.7 mm$^3$, respectively (i.e. 0.05 or 0.12% of the ball volume). In comparison the relative effective volume of the C-sphere specimen is also about 0.12% (i.e. volume efficiency). The effective surface of the notched ball specimens is about 0.95 or 1.6 mm$^2$, respectively (i.e. 1.3 or 2.2% of the balls surface). In comparison the relative effective surface of the C-sphere specimen is also in the range of 2.5% area efficiency. It should be noted that the C-sphere test has only a little higher area efficiency compared to the notched ball test, the advantage of which is outweighed practically by the very difficult and expensive machining of the C-sphere notch. In that respect the achieved gain of effective surface seems to be unspectacular and we believe that this proposed notched ball test is the more flexible and commercial solution.

Of course, the effective volume (or the effective surface, respectively) has also some influence on the strength (see Eq. (5)). In the actual case the effective volume (surface) of the specimens of set B is almost 2 times higher than that of set A and following Eq. (5) the strength should be almost 6% lower. In fact this effect is again masked by the scatter of the data and has not

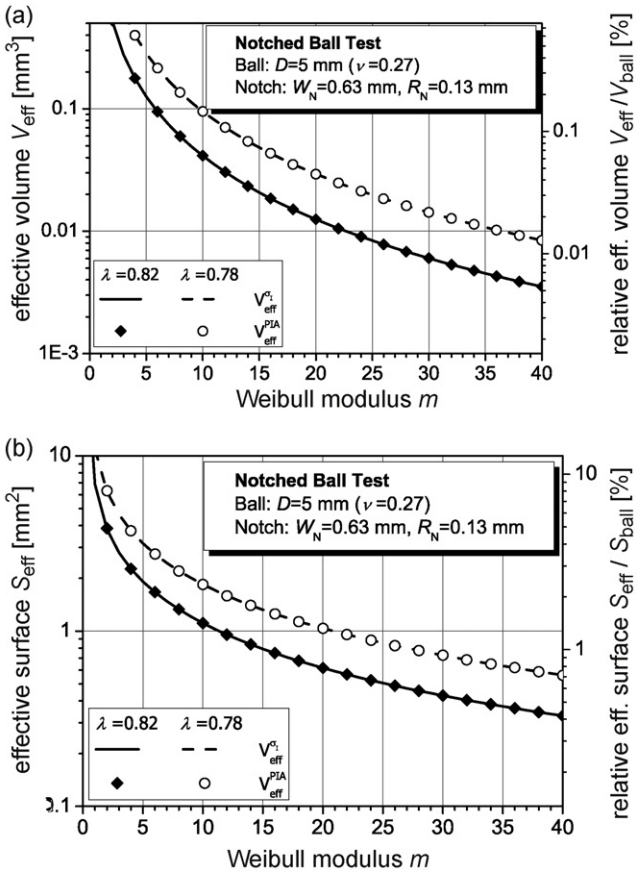


Fig. 16. Effective volume (a) and effective surface (b) versus the Weibull modulus for the notched ball specimens tested in this paper: $D = 5$ mm, $\omega = 0.13$, $\rho = 0.21$, $\lambda = 0.82$ (for set A) and $\lambda = 0.78$ (for set B). Note that specimens A and B differ by a factor of about 2 with respect to the effective volume and surface. Within each case no significant difference can be detected whether the PIA or the $\sigma_1$ criterion has been used (the symbols are centered on the corresponding lines).

been accounted for in the above data evaluation (if this effect were be taken into account the characteristic strength of sets A and B are still equal within a 90% confidence limit).

On the basis of the effective volume a prediction of the four-point bending strength of 4 mm × 3 mm × 45 mm specimens[7,15] is possible. The predicted characteristic strength is 870 MPa, which is a typical value of a commercial high quality silicon nitride material.

In summary, the data evaluation of the notched ball test give consistent results, the experiments are easy to perform and the measurement uncertainties are relatively small.

## 5. Concluding remarks

A new strength test for ceramic balls is proposed. Specimen preparation and testing procedure are relatively simple and measurement uncertainties are low. This makes the testing of even very small balls (down to a diameter of about 2 mm) possible. For the data evaluation a numerical analysis is necessary. This paper has provided some simple solutions for a restricted range of recommended notch geometries. The full results of the analysis can be found on our homepage.[24]

The strength of balls is determined to a large extent by the quality of their surface, which may also depend on machining and handling. In that sense, this strength test examines the quality of components (the balls) and can even be used to analyse damage in balls after service.

It is planned to perform experiments on bearing balls (before and after action in service) soon.

## Acknowledgements

The support of this work by the company SKF (www.skf.com) and the very helpful discussions with Hubert Köttritsch and Oskar Schöppl (both at SKF) are gratefully acknowledged.

## Appendix A

In this appendix, a general approach for the relationship between the applied force and the induced tensile stress amplitude at the ball's surface with respect to the dimension of the notched ball is developed. The geometry of the specimens is considered ideally.

The derivation of a simple formula for calculating the maximum stress is based on beam theory, since the loading situation in a Notched Ball specimen is similar to a beam with a given cross-section (i.e. circle segment) loaded by a torque $M_y$ (see Fig. 17a). There is also some compressive stress superposed, which is small compared to the effect by the torque loading. It is accounted for in the numerical analysis, but not in the following derivation.

The tensile stress in the extreme fibre of a torque-loaded beam is given by

$$\sigma_{\max}^{beam} = \frac{M_y}{I_y/y_m} \tag{8}$$

with the torque $M_y$, the moment of the area $I_y$ with respect to the neutral plane, and the distance $y_m$ of the neutral plane to the extreme fibre. This formula can be evaluated analytically for a cross-section given by a circle segment, but leads to a relatively complicated expression (see for example Ref. [33]). A much simpler expression is obtained by assuming a cross-section given by an isosceles triangle, see dashed area in Fig. 17b. $I_y$ and $y_m$ are then given by

$$I_y = \frac{ah^3}{36}, \tag{9}$$

$$y_m = \frac{2h}{3}. \tag{10}$$

Actually the derived expression is valid for the case of a long beam (i.e. the length should be in the range of 10 times the width of the beam) with a cross-section defined by an isosceles triangle. The situation in the notched ball specimen is different, since

- the cross-section is given by a circle segment, and not by an isosceles triangle;

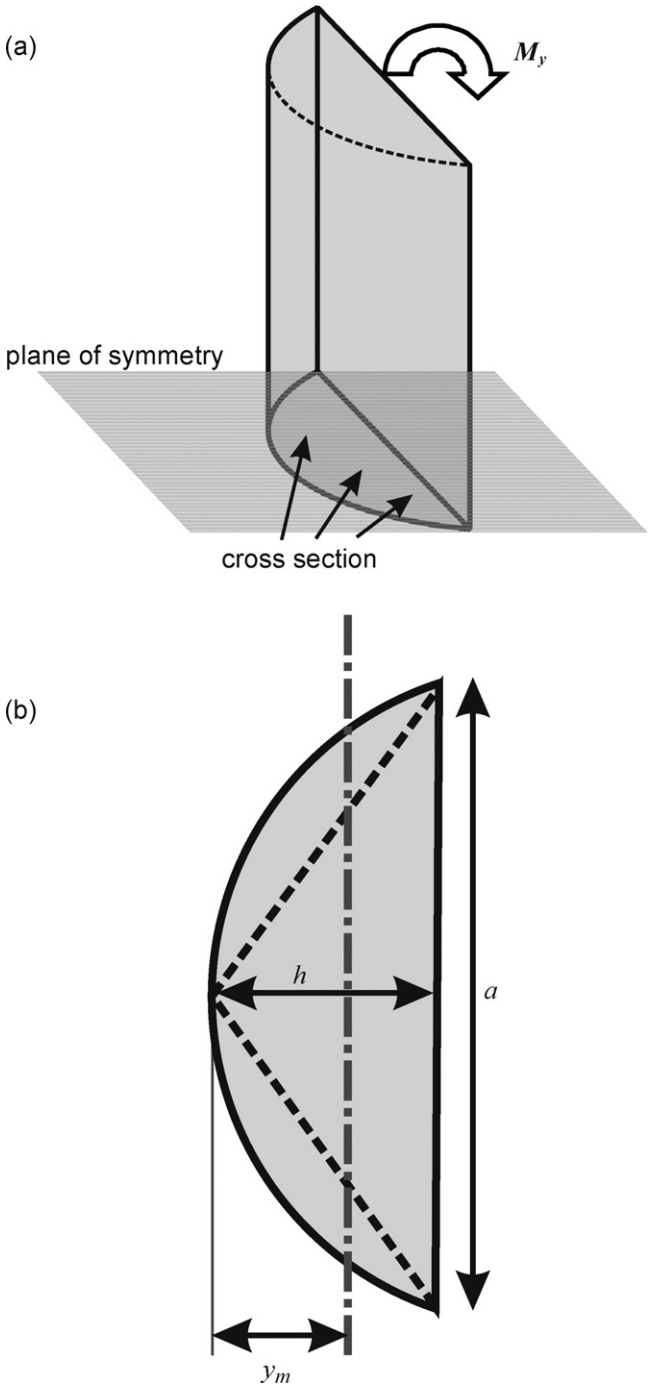


Fig. 17. Replacement model for the loaded region in the notched ball specimen: beam (a), loaded by a torque $M_y$, with the same cross-section as in the remaining ligament of the notched ball (see Fig. 2). The circle segment is defined by the segment length $a$ and the segment height $h$, see top view of the beam in (b). Since the moment of the area is a complicated expression, the circle segment is approximated by an isosceles triangle, as indicated by dashed lines (b). The neutral plane for the considered bending mode is given by the dashed–dotted line. The distance to the tensile stressed surface is $y_m = 2h/3$.

- the length of the ligament $h$ is in the order of the height $W_N$ (i.e. a very short beam!);
- the ligament has a variable cross-section with respect to the $Z$-direction: the tensile stressed surface is given by the curved surface of the ball, and the opposite area is given by the notch base with a variable fillet radius;
- the influence of Poisson's ratio is not taken into account in Eq. (8).
- there is also the effect of a superposed uniaxial compressive stress.

In order to account for all these deviations a correction factor $f$ is taken into account, namely by writing:

$$\sigma_{\max} = f\frac{M_y}{I_y/y_m} = f\frac{FR}{ah^2/24}. \tag{11}$$

The torque $M_y$ is approximately given by $M_y = R{\cdot}F$ (see Fig. 1; actually $M_y$ is given by the projected distance between force application point and the neutral plane: $R - y_m$). By taking the relationship

$$a = 2h\sqrt{\frac{D}{h} - 1} \tag{12}$$

and the definition $h = 2R - L_N = D - L_N$ into account, formula (11) can by expressed by

$$\sigma_{\max} = f\frac{6F}{h^2}\frac{1}{\sqrt[2]{(h/2R)\,(1-(h/2R))}} = f\frac{6F}{h^2}\frac{1}{\sqrt[2]{(1-\lambda)\lambda}} = f_N\frac{6F}{h^2}. \tag{13}$$

By defining a new dimensionless factor $f_N$, the expression in Eq. (2) is obtained. In this work the factor $f_N$ is defined in that way to obtain the maximum tensile stress in the equatorial plane (i.e. position 1, see Fig. 3).

## References


1. Wang, L., Snidle, R. W. and Gu, L., Rolling contact silicon nitride bearing technology: a review of recent research. *Wear*, 2000, **246**, 159–173.
2. Köttritsch, H., *Science Report: Development Centre Steyr*. Steyr: SKF Österreich AG, 2007.
3. ASTM F2094-2008, Standard specification for silicon nitride bearing balls.
4. ISO 26602-2009, Fine ceramics (advanced ceramics, advanced technical ceramics)—Silicon nitride materials for rolling bearing balls.
5. ASTM C1161-2002, Standard test method for flexural strength of advanced ceramics at ambient temperature.
6. ISO 14704-2008, Fine ceramics (advanced ceramics, advanced technical ceramics)—Test method for flexural strength of monolithic ceramics at room temperature.
7. EN843-1, Advanced Technical Ceramics, Monolithic Ceramics: Mechanical Tests at Room Temperature. Part 1—Determination of flexural strength, 1995, p. 18.
8. Supancic, P., Danzer, R., Harrer, W., Wang, Z., Witschnig, S. and Schöppl, O., Strength tests on silicon nitride balls. *Key Eng. Mater.*, 2009, **409**, 193–200.
9. Thiemeier, T., Brückner-Foit, A. and Kölker, H., Influence of fracture criterion on the failure prediction of ceramics loaded in biaxial flexure. *J. Am. Ceram. Soc.*, 1991, **74**, 48–52.
10. Munz, D. and Fett, T., *Ceramics: Mechanical Properties, Failure Behaviour, Materials Selection*. Springer Verlag, Berlin/Heidelberg/New York, 1999.
11. Börger, A., Supancic, P. and Danzer, R., The ball on three balls test for strength testing of brittle discs—stress distribution in the disc. *J. Eur. Ceram. Soc.*, 2002, **22**, 1425–1436.
12. Börger, A., Supancic, P. and Danzer, R., The ball on three balls test for strength testing of brittle discs—Part II: analysis of possible errors

in the strength determination. *J. Eur. Ceram. Soc.*, 2004, **24**, 2917–2928.
13. Quinn, G. D. and Morrell, R., Design data for engineering ceramics: a review of the flexure test. *J. Am. Ceram. Soc.*, 1991, **74**, 2037–2066.
14. Quinn, D. G., *Fractography of ceramics and glasses*. Special Publication 960-16, National Institute of Standards and Technology, 2007.
15. Danzer, R., Lube, T., Supancic, P. and Damani, R., Fracture of ceramics. *Adv. Eng. Mater.*, 2008, **10**, 275–298.
16. Köttritsch, H., *Science Report: Development Centre Steyr, 2005–2006*. Steyr: SKF Österreich AG, 2006.
17. Hertz, H., Über die Berührung fester elastischer Körper. *J. Reine Angew. Math.*, 1882, **92**, 165–171.
18. Lawn, B. R., Indentation of ceramics with spheres: a century after Hertz. *J. Am. Ceram. Soc.*, 1998, **81**, 1977–1994.
19. Fischer-Cripps, A. C. and Lawn, B. R., Stress analysis of contact deformation in quasi-plastic ceramics. *J. Am. Ceram. Soc.*, 1996, **79**, 2609–2618.
20. Lengauer, M. and Danzer, R., Silicon nitride tools for hot rolling of high alloyed steel and superalloy wires—crack growth and lifetime prediction. *J. Eur. Ceram. Soc.*, 2008, **28**, 2289–2298.
21. Wereszczak, A. A., Kirkland, T. P. and Jadaan, O. M., Strength measurement of ceramic spheres using a diametrally compressed "c-sphere" specimen. *J. Am. Ceram. Soc.*, 2007, **90**, 1843–1849.
22. ANSYS Manual: Documentation for ANSYS, Release 11, 2007.
23. ANSYS Manual: ANSYS Parametric Design Language Guide, Release 11, 2007.
24. Equation for the determination of the maximum tensile stress in notched ball specimens. Section Research, 2009, www.unileoben.ac.at/isfk.
25. EN ISO 7500-1, Metallic materials—Verification of static uniaxial testing machines—Part 1: Tension/compression testing machines—Verification and calibration of the force-measuring system.
26. OIML R 65, International recommendation: force measuring system of uniaxial material testing machines.
27. Wachtmann, J. B., *Mechanical Properties of Ceramics*. John Wiley & Sons, New York, 1996.
28. Weibull, W., *A Statistical Theory of Strength of Materials*. Royal Swedish Institute for Engineering Research, Stockholm, 1939, pp. 1–45.
29. Weibull, W., A statistical distribution function of wide applicability. *J. Appl. Mech.*, 1951, **18**, 293–298.
30. ENV 843-5, Advanced Technical Ceramics, Monolithic Ceramics, Mechanical Properties at Room Temperature, Part 5: Statistical Analysis, 1996.
31. Baratta, F. I., Quinn, G. D., and Matthews, W. T., Errors associated with flexure testing of brittle materials. Technical Report TR 87-35, July 1987, US Army Materials Technology Laboratory, Watertown, MA, USA. NTIS No. AD-A187470.
32. Lube, T., Manner, M. and Danzer, R., The miniaturisation of the 4-point bend-test. *Fatigue Fract. Eng. Mater. Struct.*, 1997, **20**, 1605–1616.
33. Gere, J. M. and Timoshenko, S. P., *Mechanics of Materials* (*3rd ed.*). Chapman & Hall, Singapore, 1991.